Eur. Phys. J. C 44, 567–576 (2005)
Digital Object Identifier (DOI) 10.1140/epjc/s2005-02273-2

THE EUROPEAN PHYSICAL JOURNAL C

J/ψ gluonic dissociation revisited: II. Hydrodynamic expansion effects

B.K. Patra[1,a], V.J. Menon[2]

[1] Department of Physics, Indian Institute of Technology, Roorkee 247 667, India
[2] Department of Physics, Banaras Hindu University, Varanasi 221 005, India

Received: 16 March 2005 /
Published online: 27 September 2005 –

Abstract. We explicitly take into account the effect of the hydrodynamic expansion profile on the gluonic break-up of the J/ψ's produced in an equilibrating parton plasma. Attention is paid to the space-time inhomogeneities as well as Lorentz frames while deriving new expressions for the gluon number density n_g, the average dissociation rate $\langle\tilde{\Gamma}\rangle$, and the survival probability of ψ, S. A novel type of partial wave interference mechanism is found to operate in the formula of $\langle\tilde{\Gamma}\rangle$. A non-relativistic longitudinal expansion from the small length of the initial cylinder is found to push the $S(p_{\rm T})$ graph above the no flow case considered by us earlier [9]. However, the relativistic flow corresponding to the large length of the initial cylinder pushes the curve of $S(p_{\rm T})$ downwards at LHC but upwards at RHIC. This mutually different effect on $S(p_{\rm T})$ may be attributed to the different initial temperatures generated at LHC and RHIC.

PACS. 12.38.Mh

1 Introduction

An extensive literature exists on the possible suppression [1–6] of the J/ψ mesons in a quark–gluon plasma and their proposed regeneration [7]. Among the well known mechanisms of J/ψ dissociation the one due to gluonic bombardment [8] deserves special attention here. Recently the present authors [9] considered the statistical mechanics of the important physical observables viz. the gluon number density, thermally-averaged g–ψ break-up rate, and the ψ meson survival probability appropriate to RHIC/LHC initial conditions. We found [9] that these observables are *significantly* affected if one employs improved expressions for the gluon distribution function, the g–ψ relative flux, and the ψ meson formation time.

Of course, it is a well-recognized fact that the longitudinal/transverse expansion of the medium controls the master rate equations [10] for the time-evolution of the plasma temperature and parton fugacities. But the literature *does not* tell how the fluid velocity profile itself influences the Lorentz transformations connecting the rest frames of the fireball, the plasma, and the ψ meson. In other words, since the *flow velocity profile* causes inhomogeneities in space-time, the scenario of the J/ψ gluonic break-up may be affected in a quite non-trivial manner and the aim of the present paper is to address this hitherto unsolved problem.

Section 2 below recalls a few aspects of relativistic hydrodynamics for the sake of ready reference. Next, a new expression for the gluon number density is derived in Sect. 3 showing how an extra dilation factor γ associated with the flow appears. Next, in Sect. 4 careful Lorentz transformations are used to calculate the flux-weighted cross section and an explicit dependence is brought out on the hydrodynamic velocity $\boldsymbol{w}$ observed in the J/ψ rest frame. Next, Sect. 5 develops the machinery for computing the J/ψ survival probability as a function of transverse momentum. Finally, Sect. 6 summarizes our main conclusions applicable to non-relativistic/relativistic flows.

2 Aspects of hydrodynamics

Preliminaries

Consider the rest frame of the hot, dense fireball produced in an ultrarelativistic heavy-ion collision. Within an initial time span $t_i = \tau_0 \sim 0.5\,\mathrm{fm}/c$ it is supposed to achieve local thermal equilibrium. The plasma now expands rapidly, gets cooled at the expense of the internal energy, and is driven towards chemical equilibration through partonic reactions. The plasma's life ends, i.e., freeze-out occurs at the instant $t_{\rm life}$ when the temperature drops to 200 MeV, say. Such a picture of collective flow is known to have a profound effect on the measured dilepton spectrum [11], the dependence of the color screening mechanism on the equation of state [12], the anisotropy in the transverse-momentum distribution [13] of the output hadrons, the

[a] e-mail: binoy@veccal.ernet.in

azimuthal asymmetry of J/ψ suppression in non-central heavy-ion collisions [14], etc.

Equation of motion

We employ the units $\hbar = c = 1$ and follow closely the hydrodynamic summary given by Pal et al. [12] based upon the *cylindrical symmetry* appropriate to central collisions. In the fireball frame a general time-space point x and the 4-velocity u of the fluid have the form

$$x = (t, \boldsymbol{x}); \qquad u = (\gamma, \gamma \boldsymbol{v}),$$
$$\gamma = \left(1 + \boldsymbol{u}^2\right)^{1/2} = \left(1 - \boldsymbol{v}^2\right)^{-1/2}, \tag{1}$$

where $\boldsymbol{v}$ is the local 3 velocity and γ is the corresponding Lorentz factor. Ignoring viscosity the conservation law for the energy-momentum tensor $T^{\mu\nu}$ reads

$$\partial_\mu T^{\mu\nu} = 0; \qquad T^{\mu\nu}(x) = (\epsilon + P) u^\mu u^\nu + P g^{\mu\nu}, \tag{2}$$

where the energy density ϵ and pressure P are supposed to be measured in a frame comoving with the plasma. The relationship between *the fireball usual time t and medium proper time τ* is, of course,

$$\frac{\mathrm{d}\tau}{\mathrm{d}t} = \frac{1}{\gamma}; \qquad t_i \le t \le t_{\mathrm{life}}. \tag{3}$$

Longitudinal expansion

In Bjorken's boost-invariant one-dimensional flow the profile admits a simple *analytical* solution:

$$\boldsymbol{v} = \frac{z}{t}\hat{e}_z; \qquad \tau = \left(t^2 - z^2\right)^{1/2} \ge \tau_0, \tag{4}$$

where $\hat{e}_z$ is a unit vector along the collision axis. The corresponding temperature $T \propto \tau^{-1/3}$ is known to fall rather slowly, e.g. in the case of gold nuclei colliding at RHIC. Hence the J/ψ suppression remains comparatively high via the color screening/gluonic dissociation mechanisms.

Transverse expansion

As summarized in [11, 12] the 4-velocity profile becomes quite intricate and a numerical integration of the dynamical equations (2) and (3) becomes very hard in the case of a $3+1$-dimensional expansion. For our purpose it will suffice to assume that the collective flow occurs only along the lateral directions without rotation as given by the *empirical* ansatz

$$\boldsymbol{v} = \frac{r}{t}\hat{e}_r; \qquad \tau = \left(t^2 - r^2\right)^{1/2}, \tag{5}$$

where $\hat{e}_r$ is the unit vector along $\boldsymbol{r}$ in a cylindrical coordinate system (r, z, ϕ). It is known from the numerical solution of (2) that a transverse flow causes very rapid cooling in the case of lead nuclei colliding at LHC. Hence the J/ψ survival probability becomes relatively high via the color screening/gluonic dissociation scenarios. We now proceed to formulate the statistical mechanics of some physical observables following closely the logic of [9].

3 Gluon number density

Preliminaries

Working in the fireball rest frame and assuming local thermal equilibrium let the symbol x denote a typical time-space point, u the medium 4-velocity, T the absolute temperature, $K = (K^0, \boldsymbol{K})$ the gluon 4-momentum, 16 the spin-color degeneracy factor, λ_g the gluon fugacity, f the one-body Bose–Einstein distribution function, and n_g the gluon number density given mathematically by

$$f = \frac{\lambda_g}{\mathrm{e}^{K\cdot u/T} - \lambda_g}; \qquad n_g(x) = 16 \int \frac{\mathrm{d}^3\boldsymbol{K}}{(2\pi)^3} f. \tag{6}$$

It may be noted that generally $\lambda_g < 1$ for a chemically unequilibrated plasma and the calculation of $K\cdot u$ is tedious in the fireball frame.

Comoving frame

If $k = (k^0, \boldsymbol{k})$ is the gluon 4-momentum in the local rest frame of the plasma, then by Lorentz transformation

$$K \cdot u = k^0; \qquad K^0/k^0 = \gamma\left(1 + \boldsymbol{v}\cdot\hat{k}\right), \tag{7}$$

where γ, $\boldsymbol{v}$ refer to the fluid motion of (1) and $\hat{k}$ is a unit vector along $\boldsymbol{k}$. Substitution into (6) simplifies the distribution function to

$$f = \frac{\lambda_g}{\mathrm{e}^{k^0/T} - \lambda_g} = \sum_{n=1}^{\infty} \lambda_g^n \, \mathrm{e}^{-nk^0/T}. \tag{8}$$

Also, upon taking the polar axis for integration along $\hat{v}$ and writing $\boldsymbol{v}\cdot\hat{k} = |\boldsymbol{v}|\cos\theta_{kv}$ our number density reduces to

$$n_g(x) = 16 \int \frac{\mathrm{d}^3k}{(2\pi)^3} \frac{K^0}{k^0} f \tag{9}$$

$$= \frac{2}{\pi^3} \int_0^\infty \mathrm{d}k^0 k^{0\,2} \int_{-1}^{1} \mathrm{d}\cos\theta_{kv} \tag{10}$$

$$\times \int_0^{2\pi} \mathrm{d}\phi_{kv}\ \gamma\left(1 + |\boldsymbol{v}|\cos\theta_{kv}\right) \sum_{n=1}^{\infty} \lambda_g^n \mathrm{e}^{-nk^0/T}$$

$$= \frac{16}{\pi^2}\gamma T^3 \sum_{n=1}^{\infty} \frac{\lambda_g^n}{n^3}. \tag{11}$$

Remarks

This result is *new* and shows in a compact manner how the number density depends upon γ, T, and λ_g (although these dependences are generally interwoven through the evolution equations). It may be stressed that in spite of the occurrence of a $\boldsymbol{v}\cdot\hat{k}$ term in (7) our final n_g depends on $\boldsymbol{v}^2$ through γ. Our equation (11) generalizes an earlier expression obtained by Xu et al. [8] who ignored the flow velocity $\boldsymbol{v}$ completely and worked with a factorized form of the Bose–Einstein distribution containing λ_g only in the numerator.

Table 1. Initial values for the time, temperature, fugacities etc. at RHIC(1), LHC(1) only [15]

	T (GeV)	$t_i = \tau_0$ (fm)	λ_g	λ_q	$n_g^{v=0.1c}$ $(\mathrm{fm})^{-3}$	$n_g^{v=0.9c}$ $(\mathrm{fm})^{-3}$
RHIC(1)	0.55	0.70	0.05	0.008	1.78	4.05
LHC(1)	0.82	0.5	0.124	0.02	14.73	33.63

Numerical estimate at t_i

The behavior of (11) can be easily studied at the instant when the thermalized fireball was formed in a high energy heavy-ion collision. The initial conditions predicted by HIJING Monte Carlo simulations are summarized in Table 1.

There the gluon densities computed via (11) in the non-relativistic ($v \approx 0.1c$) and ultrarelativistic ($v \approx 0.9c$) regions are also listed, showing a relative enhancement by the factor

$$\frac{n_{gi}^{v=0.9c}}{n_{gi}^{v=0.1c}} \approx \frac{(1-0.01)^{1/2}}{(1-0.81)^{1/2}} \approx 2.28. \tag{12}$$

Temporal evolution

It is very tedious to employ the exact distribution function f of (6) for determining how the fugacities and temperature evolve with the proper time τ of the medium. Hence we shall directly borrow the master rate equations from the existing literature based upon an approximately *factorized* form of f. It is plausible that we may assume that such an approximation will not markedly affect our final conclusions, since $\lambda_g < 1$. For a longitudinal expansion parametrized by (4) the relevant ordinary differential equations [10] are known to be

$$\frac{\dot{\lambda_g}}{\lambda_g} + 3\frac{\dot{T}}{T} + \frac{1}{\tau} = R_3\,(1-\lambda_g) - 2R_2\left(1 - \frac{\lambda_g^2}{\lambda_q^2}\right),$$

$$\frac{\dot{\lambda_q}}{\lambda_q} + 3\frac{\dot{T}}{T} + \frac{1}{\tau} = R_2\,\frac{a_1}{b_1}\left(\frac{\lambda_g}{\lambda_q} - \frac{\lambda_q}{\lambda_g}\right),$$

$$\left(\lambda_g + \frac{b_2}{a_2}\lambda_q\right)^{3/4} T^3\tau = \text{const.} \tag{13}$$

Here λ_q (λ_g) is the quark (gluon) fugacity, N_f the number of flavors, and the remaining symbols are defined by

$$\begin{aligned} R_2 &= 0.5 n_g \langle v\sigma_{gg\longrightarrow q\bar{q}}\rangle, & R_3 &= 0.5 n_g \langle v\sigma_{gg\longrightarrow ggq}\rangle, \\ a_1 &= 16\zeta(3)/\pi^2, & a_2 &= 8\pi^2/15, \\ b_1 &= 9\zeta(3)N_f/\pi^2, & b_2 &= 7\pi^2 N_f/20. \end{aligned} \tag{14}$$

Next, for the transverse expansion parametrized by (5) the appropriate partial differential equations [12] read

$$\partial_\tau T^{00} + r^{-1}\partial_r\left(rT^{01}\right) + \tau^{-1}\left(T^{00}+P\right) = 0 \tag{15}$$

and

$$\partial_\tau T^{01} + r^{-1}\partial_r\left[r\left(T^{00}+P\right)v_r^2\right] + \tau^{-1}T^{01} + \partial_r P = 0, \tag{16}$$

where

$$T^{00} = (\epsilon + P)u^0u^0 - P. \tag{17}$$

Their solutions on the computer yield the functions $T(x)$, $\lambda_g(x)$ and hence $n_g(x)$, subject to the stated initial conditions.

4 Thermally-averaged rate

Preliminaries

Next, we turn to the question of applying statistical mechanics to gluonic break-up of the J/ψ moving inside an expanding parton plasma. In the fireball frame consider a ψ meson of mass m_ψ, 4-momentum $p_\psi = (p_\psi^0, \boldsymbol{p}_\psi)$, 3-velocity $\boldsymbol{v}_\psi$ and dilation factor γ_ψ defined by

$$\boldsymbol{v}_\psi = \boldsymbol{p}_\psi/p_\psi^0, \qquad \gamma_\psi = p_\psi^0/m_\psi = \left(1 - \boldsymbol{v}_\psi{}^2\right)^{-1/2}. \tag{18}$$

The invariant quantum mechanical dissociation rate Γ for a g–ψ collision may be written compactly as

$$\Gamma = v_{\mathrm{rel}}\sigma, \tag{19}$$

where v_{rel} is the relative flux and σ the cross section measured in any chosen frame. Its thermal average over gluon momentum in the *fireball* frame reads

$$\langle\Gamma(x)\rangle = \frac{16}{n_g(x)}\widetilde{\int}\frac{\mathrm{d}^3K}{(2\pi)^3}\;\Gamma f. \tag{20}$$

Here the tilde implies that the gluon is hard enough to break J/ψ and the gluonic distribution function f is evaluated at the *location* of the ψ meson viz. at the time-space point

$$x = (t, \boldsymbol{x}_\psi)\,. \tag{21}$$

The highly non-trivial integral (20) is best handled in the ψ meson rest frame by generating several useful pieces of kinematic information as follows.

Kinematics in J/ψ rest frame

Let $q = (q^0, \boldsymbol{q})$ be the gluon 4-momentum measured in the ψ meson *rest* frame. Since the relative flux becomes $v_{\mathrm{rel}}^{\mathrm{Rest}} = c = 1$, our invariant Γ reduces to the QCD-based cross section [16]

$$\begin{aligned} \Gamma = \sigma_{_{\mathrm{Rest}}} &= B\big(Q^0-1\big)^{3/2}/{Q^0}^5; \qquad q^0 \geq \epsilon_\psi, \\ Q^0 &= \frac{q^0}{\epsilon_\psi} \geq 1; \qquad B = \frac{2\pi}{3}\left(\frac{32}{3}\right)^2\frac{1}{m_c(\epsilon_\psi m_c)^{1/2}}, \end{aligned} \tag{22}$$

where ϵ_ψ is the J/ψ binding energy and m_c the charmed quark mass. This $\sigma_{\rm Rest}$ possesses a sharp peak at the gluon energy

$$q_p^0 = \frac{10\epsilon_\psi}{7} = 0.92\,{\rm GeV}; \quad Q_p^0 = \frac{10}{7}. \tag{23}$$

Also, the energy variable for the massless gluon transforms via

$$K^0 = \gamma_\psi \left(q^0 + \boldsymbol{v}_\psi \cdot \boldsymbol{q}\ \right) = \gamma_\psi q^0 \left(1 + |\boldsymbol{v}_\psi| \cos\theta_{q\psi}\right), \tag{24}$$

with $\theta_{q\psi}$ being the angle between the $\hat{q}$ and $\hat{v}_\psi$ unit vectors. Furthermore, the fluid 4-velocity $w = (w^0, \boldsymbol{w})$ seen in the ψ rest frame will be explicitly given by the Lorentz transformations

$$w^0 = \gamma_\psi \left(u^0 - \boldsymbol{u}\cdot\boldsymbol{v}_\psi\right) = \gamma_\psi\gamma\left(1 - \boldsymbol{v}\cdot\boldsymbol{v}_\psi\right), \tag{25}$$

$$\begin{aligned}\boldsymbol{w} &= \Big[\ \boldsymbol{u} - (\boldsymbol{u}\cdot\hat{v}_\psi)\,\hat{v}_\psi\ \Big] + \gamma_\psi\left[(\boldsymbol{u}\cdot\hat{v}_\psi) - u^0|\boldsymbol{v}_\psi|\right]\hat{v}_\psi \\ &= \gamma\left[\boldsymbol{v} - \gamma_\psi\boldsymbol{v}_\psi + (\gamma_\psi - 1)\,(\boldsymbol{v}\cdot\hat{v}_\psi)\,\hat{v}_\psi\right]. \end{aligned}\tag{26}$$

Finally, the scalar product is

$$K\cdot u = q\cdot w = q^0 w^0 - q^0|\boldsymbol{w}|\cos\theta_{qw}, \tag{27}$$

where θ_{qw} is the angle between $\hat{q}$ and $\hat{w}$. We thus have all the ingredients needed to calculate the thermally-averaged rate of (20).

Evaluation of $\langle \Gamma(x)\ \rangle$

Upon taking the polar axis for the $\boldsymbol{q}$ integration along $\hat{v}_\psi$, denoting the solid angle element by ${\rm d}\Omega_{q\psi}$, and expanding f in a power series, we can write

$$\langle\Gamma(x)\rangle = \frac{16}{n_g}\int\frac{{\rm d}^3q}{(2\pi)^3}\,\frac{K^0}{q^0}\,\sigma_{\rm Rest}\sum_{n=1}^{\infty}\lambda_g^n {\rm e}^{-nK\cdot u/T} \tag{28}$$

$$\begin{aligned}&= \frac{2}{\pi^3 n_g}\int_{\epsilon_\psi}^{\infty}{\rm d}q^0 {q^0}^2\int_0^{4\pi}{\rm d}\Omega_{q\psi}\gamma_\psi\left(1 + |\boldsymbol{v}_\psi|\cos\theta_{q\psi}\right) \\ &\quad\times\sigma_{\rm Rest}\sum_{n=1}^{\infty}\lambda_g^n {\rm e}^{-nq\cdot w/T}. \end{aligned}\tag{29}$$

This integral is performed in the appendix based on the following nomenclature.

Symbols/notation

Using the nomenclature in the fireball frame we define

$$\begin{aligned}&(\theta_v, \phi_v) = \text{polar angles of } \hat{v};\\ &(\theta_{v_\psi}, \phi_{v_\psi}) = \text{polar angles of } \hat{v}_\psi,\\ &F = \boldsymbol{v}\cdot\hat{v}_\psi\\ &\quad = |\boldsymbol{v}|\left[\sin\theta_v\sin\theta_{v_\psi}\cos(\phi_v - \phi_{v_\psi}) + \cos\theta_v\cos\theta_{v_\psi}\right],\\ &Y = \gamma_\psi|\boldsymbol{v}_\psi| - (\gamma_\psi - 1)F,\\ &w^0 = \gamma\gamma_\psi(1 - F|\boldsymbol{v}_\psi|); \qquad \boldsymbol{w} = \gamma\left(\boldsymbol{v} - Y\hat{v}_\psi\right),\\ &|\boldsymbol{w}| = \left[|\boldsymbol{w}|^2\right]^{1/2} = \gamma\Big[|\boldsymbol{v}|^2 + Y^2 - 2YF\Big]^{1/2},\\ &\theta_{\psi w} = \text{angle between } \hat{v}_\psi \text{ and } \hat{w},\\ &\cos\theta_{\psi w} = \frac{1}{|\boldsymbol{w}|}\,(\boldsymbol{w}\cdot\hat{v}_\psi) = \frac{1}{|\boldsymbol{w}|}(F - Y). \end{aligned}\tag{30}$$

Also will be needed

$$\begin{aligned}Q^0 &= q^0/\epsilon_\psi; \qquad C_n = n\epsilon_\psi w^0/T,\\ D_n &= n\epsilon_\psi|\boldsymbol{w}|/T; \qquad \rho_n = D_n Q^0,\\ A_n^\pm &= C_n \pm D_n = n\epsilon_\psi\left(w^0 \pm |\boldsymbol{w}|\right)/T,\\ I_0(\rho_n) &= \sinh(\rho_n)/\rho_n,\\ I_1(\rho_n) &= \cosh(\rho_n)/\rho_n - \sinh(\rho_n)/\rho_n^2,\\ nK\cdot u/T &= nq\cdot w/T = C_n Q^0 - \rho_n\cos\theta_{qw}. \end{aligned}\tag{31}$$

Result of integration

From (A.4) we find

$$\begin{aligned}\langle\Gamma(x)\rangle = \frac{8\epsilon_\psi^3\gamma_\psi}{\pi^2 n_g}\sum_{n=1}^{\infty}\lambda_g^n\int_1^{\infty}{\rm d}Q^0{Q^0}^2\sigma_{\rm Rest}\left(Q^0\right){\rm e}^{-C_n Q^0},\\ \times\Big[\ I_0(\rho_n) + I_1(\rho_n)|\boldsymbol{v}_\psi|\cos\theta_{\psi w}\ \Big]. \end{aligned}\tag{32}$$

By decomposing the hyperbolics I_0 and I_1 into exponentials this result can also be expressed as

$$\begin{aligned}\langle\Gamma(x)\rangle = \frac{4\epsilon_\psi^2 T\gamma_\psi}{\pi^2|\boldsymbol{w}|n_g}\sum_{n=1}^{\infty}\frac{\lambda_g^n}{n}\int_1^{\infty}{\rm d}Q^0 Q^0\sigma_{\rm Rest}\left(Q^0\right)\\ \times\Big[\Big(\ 1 + \boldsymbol{v}_\psi\cdot\hat{w}(1 - 1/\rho_n)\ \Big){\rm e}^{-A_n^- Q^0}\\ -\Big(\ 1 - \boldsymbol{v}_\psi\cdot\hat{w}(1 + 1/\rho_n)\ \Big){\rm e}^{-A_n^+ Q^0}\Big]. \end{aligned}\tag{33}$$

Remarks

The expressions (32) and (33) are original and demonstrate how the mean dissociation rate $\langle\Gamma(x)\rangle$ depends on the *hydrodynamic* flow through $|\boldsymbol{w}|$ (or w^0) as well as the angle $\theta_{\psi w}$ in the notation of (30). The structure of $\exp(\pm D_n Q^0)$ tells us that a numerical treatment of (32) is convenient if $0 \le |\boldsymbol{w}| \le T/\epsilon_\psi$ while that of (33) is suitable if $T/\epsilon_\psi \le |\boldsymbol{w}| \le \infty$. From the analytical viewpoint it is much more advisable to work with the modified rate

$$\langle\tilde{\Gamma}(x)\rangle \equiv n_g(x)\langle\Gamma(x)\rangle. \tag{34}$$

This is because $\langle\tilde{\Gamma}\rangle$ is devoid of any n_g factor appearing in the denominator of (32). Furthermore, $\langle\tilde{\Gamma}\rangle$ will be seen to enter directly in the survival probability ${\rm e}^{-W}$ in (51) later.

Analytical estimate

The physical interpretation of our graphs below will be facilitated by deriving a rough approximation for $\langle\tilde{\Gamma}\rangle$ as follows. In (32) we retain only the $n = 1$ term of the summation, and approximate the integrand by its peak value at Q_p^0 (cf. (23)) so that the desired estimate of (34) becomes

$$\langle\tilde{\Gamma}(x)\rangle \approx \frac{8\epsilon_\psi^3\gamma_\psi}{\pi^2}\ \lambda_g \int_1^\infty \mathrm{d}Q^0 {Q^0}^2 \sigma_{\mathrm{Rest}}\ H$$
$$\propto \lambda_g\gamma_\psi H. \qquad (35)$$

Here the *entire* dependence on the flow velocity w is contained in the function

$$H \equiv \mathrm{e}^{-C_1 Q_p^0}\left[\ I_0\left(D_1 Q_p^0\right) + I_1\left(D_1 Q_p^0\right) \mid \boldsymbol{v}_\psi \mid \cos\theta_{\psi w}\ \right], \qquad (36)$$

with the coefficients C_1, D_1 and $A_1^\pm$ read off from (31). We are now ready to discuss some consequences of (35) in *three* cases, viz., a static medium in the fireball frame, no flow in the J/ψ rest frame, and ultrarelativistic flow in either frame.

Static medium in fireball frame

Remembering the notation of (30) and (31) consider the *hypothetical* case

$$\boldsymbol{v} = \boldsymbol{0};\quad \gamma = 1;\quad F = 0;\quad Y = \gamma_\psi|\boldsymbol{v}_\psi|,$$
$$w^0 = \gamma_\psi;\quad \boldsymbol{w} = -\gamma_\psi\boldsymbol{v}_\psi;\quad C_n = n\epsilon_\psi\gamma_\psi/T, \qquad (37)$$
$$\cos\theta_{\psi w} = -1,\quad D_n = C_n|\boldsymbol{v}_\psi|;\quad A_n^\pm = C_n(1 \pm |\boldsymbol{v}_\psi|).$$

This is precisely the case treated in our earlier paper [9] where the g–ψ relative flux was correctly taken in the ψ meson rest frame. Equations (32) and (33) also improve the work of Xu et al. [8] in which one had written the g–ψ relative flux in the fireball frame. Figures 1 and 2 borrowed from [9] display the temperature and transverse momentum dependence of the *usual* rate $\langle\Gamma\rangle$ based on (32) and (33) relevant to the LHC(1) initial fugacity λ_{gi}. For the sake of comparison the corresponding curves of the *modified* rate $\langle\tilde{\Gamma}\rangle$ using (34) are drawn in Figs. 3 and 4. Due to the assumed absence of flow there is no inhomogeneity with respect to x and the J/ψ formation time is also ignored at this stage. Various features of the indicated diagrams are interpreted in the next paragraph.

Interpretation

(i) Following the arguments given by Xu et al. [8] it is known that the peak of σ_{Rest} at Q_p^0 gives a rich structure to the usual rate $\langle\Gamma\rangle$ in Figs. 1 and 2.

(ii) However, the modified rate $\langle\tilde{\Gamma}\rangle$ in Figs. 3 and 4 becomes structureless, i.e., monotonic. This is because the gluon number density n_g in (11) contains a crucial T^3 factor which changes from a low value, viz. 0.008 at $T = 0.2$ GeV, to a high value, viz. 1.0 at $T = 1$ GeV. Such a T^3 coefficient matters a lot in the conversion of $\langle\Gamma\rangle$ to $\langle\tilde{\Gamma}\rangle$ via (34).

(iii) At fixed p_{T} the steady *increase* of $\langle\tilde{\Gamma}\rangle$ with T in Fig. 3 is caused by the growing $\exp\left(-A_1^\pm Q_p^0\right)$ factors of the estimate (35) and (36).

(iv) At fixed T the monotonic *decrease* of $\langle\tilde{\Gamma}\rangle$ with p_{T} in Fig. 4 has a very interesting explanation. For the situation (37) under study $\boldsymbol{w} = -\gamma_\psi\boldsymbol{v}_\psi$ is antiparallel to $\boldsymbol{v}_\psi$ so that $\cos\theta_{\psi w} = -1$. Hence the partial wave terms I_0 and I_1 of H (36) *interfere* destructively in Fig. 4 making $\langle\tilde{\Gamma}\rangle$ small as $\mid \boldsymbol{v}_\psi \mid$ grows.

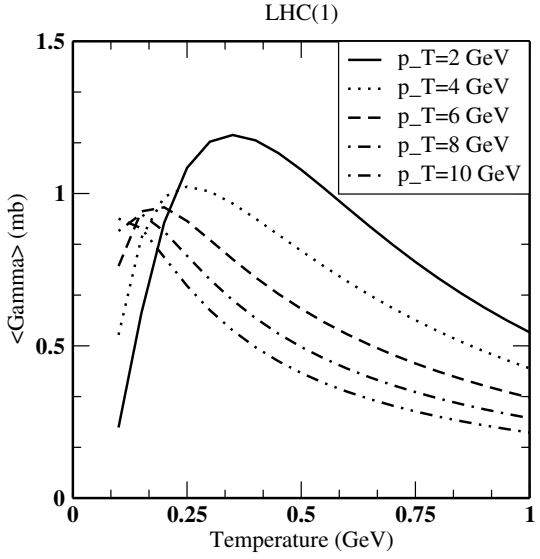

Fig. 1. The thermal-averaged gluon–ψ dissociation cross section $\langle\Gamma\rangle \equiv \langle v_{\mathrm{rel}}\sigma\rangle$ as a function of temperature at different transverse momenta p_{T} as in (19) of [9], i.e., in the absence of longitudinal flow. The initial gluon fugacity is given in Table 1 at LHC energy

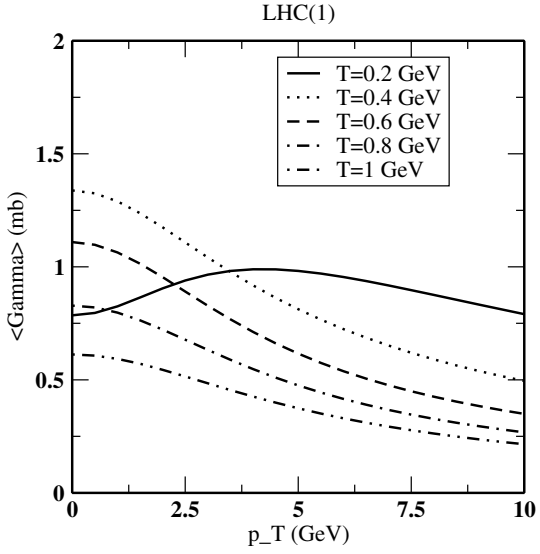

Fig. 2. The variation of $\langle\Gamma\rangle \equiv \langle v_{\mathrm{rel}}\sigma\rangle$ with transverse momentum at different temperatures [9] as in Fig. 1 in the absence of a flow profile

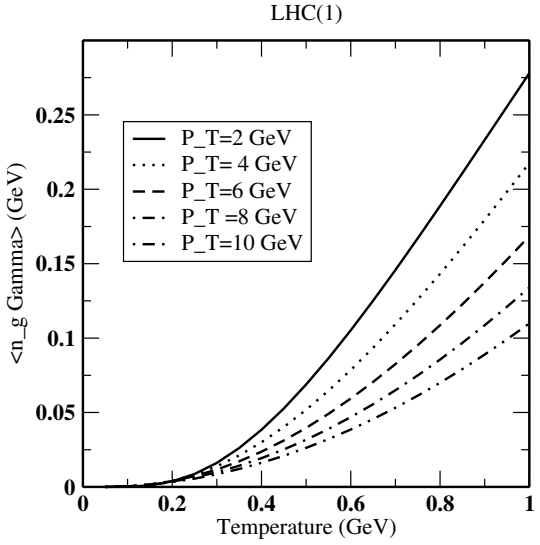

Fig. 3. The variation of the *modified* rate $\langle\tilde{\Gamma}\rangle \equiv n_g\langle\Gamma\rangle$ with temperature at different values of transverse momentum corresponding to $\langle\Gamma\rangle$ of Fig. 1 is depicted here

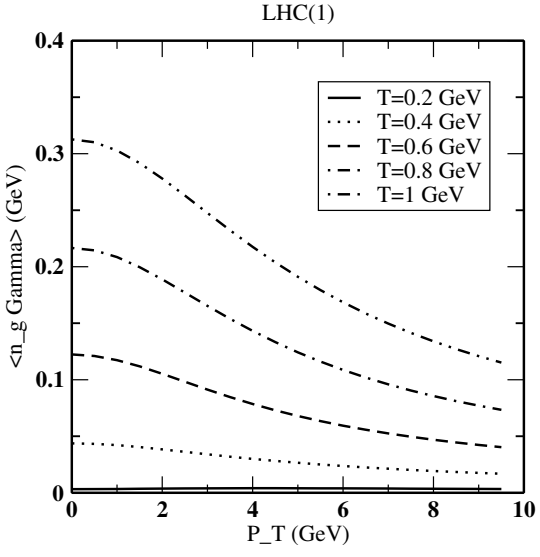

Fig. 4. The variation of the *modified* rate $\langle\tilde{\Gamma}\rangle \equiv n_g\langle\Gamma\rangle$ with transverse momentum at different values of temperatures corresponding to $\langle\Gamma\rangle$ of Fig. 2 is shown here in the absence of flow

No flow in J/ψ rest frame

Next, consider a configuration in the fireball frame such that the 3-velocities of the plasma and ψ meson coincide at some x. This is possible if, for example, both the fluid and ψ are moving in the transverse direction. Then in (30) and (31) we put

$$\boldsymbol{v} = \boldsymbol{v}_\psi; \qquad F = |\boldsymbol{v}_\psi|; \qquad w^0 = 1; \qquad \boldsymbol{w} = \boldsymbol{0}, \tag{38}$$
$$C_n = n\epsilon_\psi/T; \qquad \rho_n = 0; \qquad I_0(\rho_n) = 1; \qquad I_1(\rho_n) = 0.$$

Inserting this information into the exact formulae (32) and (34) and attaching a suffix 0 we find

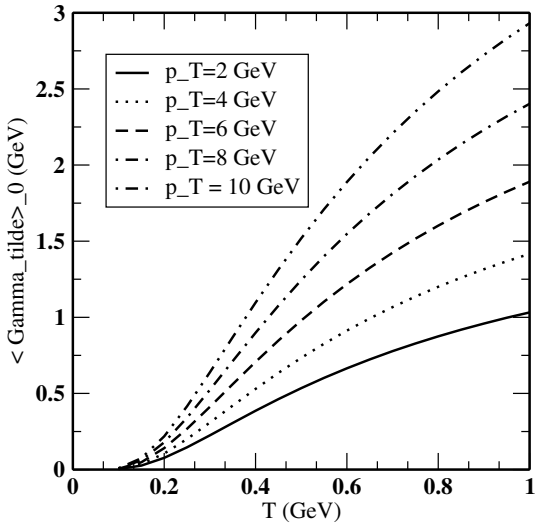

Fig. 5. The variation of the *modified* rate $\langle\tilde{\Gamma}(x)\rangle_0$ from (39) with temperature for different $p_{\rm T}$'s, when the fluid 3-velocity $\boldsymbol{w}$ in the ψ meson rest frame is zero

$$\langle\tilde{\Gamma}(x)\rangle_0 = \frac{8\epsilon_\psi^3\gamma_\psi}{\pi^2}\sum_{n=1}^{\infty}\lambda_g^n\ \mathrm{e}^{-n\epsilon_\psi/T}\int_1^\infty \mathrm{d}Q^0\ {Q^0}^2\sigma_{\rm Rest}. \tag{39}$$

Its variations with T and $p_{\rm T}$ are displayed in Figs. 5 and 6, relevant to the LHC(1) initial fugacity. The crude proportionality (35) now reduces to

$$\langle\tilde{\Gamma}(x)\rangle_0 \propto \lambda_g\gamma_\psi \mathrm{e}^{-\epsilon_\psi/T}, \tag{40}$$

which is utilized below to explain some features of the graphs.

Interpretation

(i) At fixed $p_{\rm T}$ our $\langle\tilde{\Gamma}(x)\rangle_0$ of Fig. 5 rises monotonically with T in analogy with the earlier Fig. 3. This is caused by the $\mathrm{e}^{-\epsilon_\psi/T}$ factor present in the estimate (40).
(ii) At fixed T our $\langle\tilde{\Gamma}(x)\rangle_0$ of Fig. 6 grows steadily with $p_{\rm T}$ in contrast to the earlier Fig. 4. Such a behavior is due to the coefficient γ_ψ occurring in (40).
(iii) The curves of Figs. 5 and 6 are consistently *higher* than those of Figs. 3 and 4. The reason is that there is no $I_1(\rho_n)$ term present in (39) to interfere destructively with the $I_0(\rho_n)$ term in view of the restriction (38).

Ultrarelativistic flow in either frame

Finally, suppose that at a point x in the fireball frame the medium is flowing ultrarelativistically ($|\ \boldsymbol{v}\ | \to 1$) and the J/ψ is moving slowly ($|\boldsymbol{v}_\psi| < 1/10$, say). In the ψ meson rest frame the Lorentz transformation (26) shows that $\boldsymbol{w}$ almost equals $\gamma\boldsymbol{v}$ so that $\cos\theta_{\psi w} \to \hat{v}_\psi \cdot \hat{v}$. Hence, in the case of a pure transverse expansion of the plasma $\cos\theta_{\psi w}$ can even become $+1$, implying constructive interference between the I_0 and I_1 terms of (36); this possibility will, however, be discussed in a future communication. At

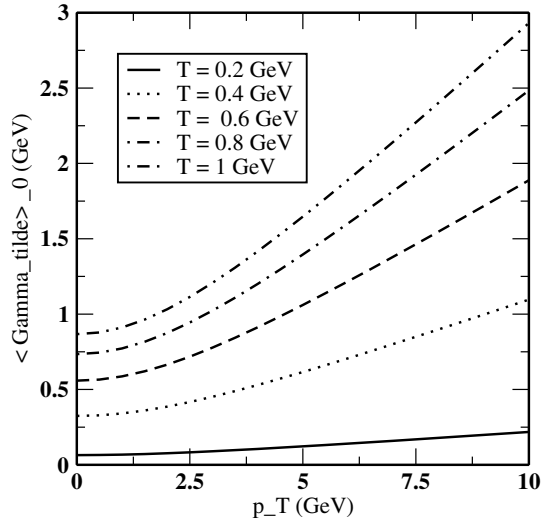

Fig. 6. The variation of the *modified* rate $\langle\tilde{\Gamma}(x)\rangle_0$ from (39) with $p_{\rm T}$'s for different values of T when the fluid 3-velocity $\boldsymbol{w}$ in the ψ meson rest frame is zero

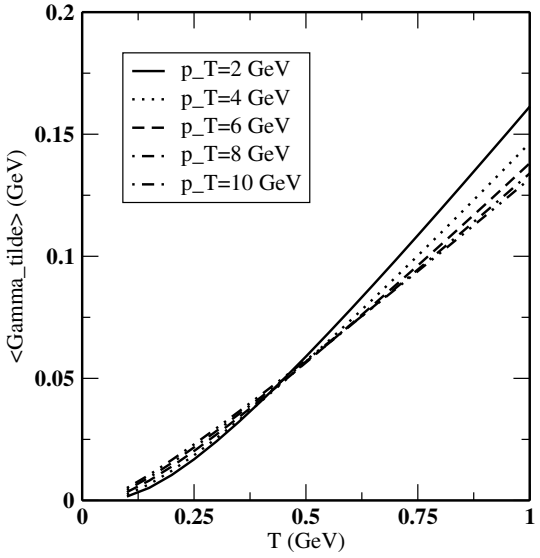

Fig. 7. The variation of the *modified* rate $\langle\tilde{\Gamma}(x)\rangle$ using (32) and (34) as a function of temperature at different transverse momenta for the ultrarelativistic longitudinal flow velocity, $v = 0.9c$

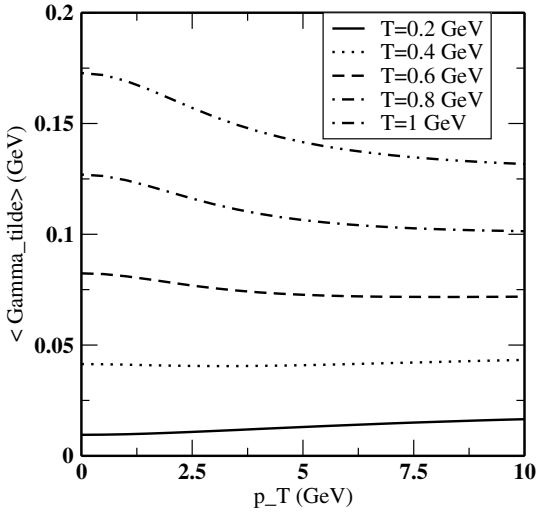

Fig. 8. The variation of the *modified* rate $\langle\tilde{\Gamma}(x)\rangle$ using (32) and (34) as a function of $p_{\rm T}$ at different values of temperatures as in Fig. 7 corresponding to ultrarelativistic longitudinal flow velocity, $v = 0.9c$

present, we illustrate the case of both the J/ψ and plasma moving ultrarelativistically (in the transverse and longitudinal directions, respectively) subject to the following kinematic conditions:

$$\begin{aligned}
&\boldsymbol{v} = 0.9\hat{e}_z; \quad \gamma = 2.3; \quad F = 0; \quad Y = \gamma_\psi|\boldsymbol{v}_\psi|,\\
&w^0 = \gamma\gamma_\psi \gg 1; \qquad |\boldsymbol{w}| \approx \gamma\gamma_\psi - \frac{1}{2\gamma\gamma_\psi},\\
&\cos\theta_{\psi w} = -\frac{Y}{|\boldsymbol{w}|} \approx -\frac{1}{\gamma};\\
&D_1 = \epsilon_\psi|\boldsymbol{w}|/T \sim \frac{\epsilon_\psi\gamma\gamma_\psi}{T} \gg 1,\\
&A_1^- = \frac{\epsilon_\psi}{T}\left(w^0 - |\boldsymbol{w}|\right) \approx \frac{\epsilon_\psi}{2T\gamma\gamma_\psi}. \qquad (41)
\end{aligned}$$

Then $I_0(\rho_1) \to I_1(\rho_1) \to \exp(\rho_1)/2\rho_1$ so that our rough estimates (35) and (36) become

$$\langle\tilde{\Gamma}(x)\rangle \propto \frac{\lambda_g T}{\gamma}\exp\left(-\frac{\epsilon_\psi Q_p^0}{2T\gamma\gamma_\psi}\right)\left[1 - \frac{|\boldsymbol{v}_\psi|^2}{\gamma}\right]. \qquad (42)$$

This information will be utilized below for explaining the main features of the graphs.

Interpretation

(i) For fixed $p_{\rm T}$, v, the exponential in (42) tends to 0 as $T \to 0$ and tends to 1 as $T \to \infty$. Therefore, the growing trend of $\langle\tilde{\Gamma}(x)\rangle$ with T in Fig. 7 is unstable.
(ii) At fixed T, v the rich behavior of $\langle\tilde{\Gamma}(x)\rangle$ with $p_{\rm T}$ in Fig. 8 arises from a sensitive competition between the bracketed factors of (42).
(iii) More precisely, at lower temperatures $T \le 0.4\,{\rm GeV}$ the exponential factor in (42) increases dominantly with $p_{\rm T}$, causing $\langle\tilde{\Gamma}(x)\rangle$ to grow.
(iv) But at higher temperatures $T \ge 0.8\,{\rm GeV}$ the third bracket in (42) decreases prominently with $p_{\rm T}$, causing $\langle\tilde{\Gamma}\rangle$ to drop.
(v) Comparison of Figs. 3 and 4 with Figs. 7 and 8 tells that the $p_{\rm T}$-dependence of $\langle\tilde{\Gamma}\rangle$ (unlike its T dependence) is quite sensitive to the non-relativistic/ultrarelativistic nature of flow in the fireball frame.

5 J/ψ survival probability

Next, we ask the important question as to how the explicit collective flow profile affects the birth and death scenarios of ψ mesons within a quark–gluon plasma. Below we consider

only *longitudinal* expansion; the case of transverse flow will be dealt with in a future communication.

Pure longitudinal expansion

Suppose at a general instant t in the fireball frame the plasma is contained inside a *cylinder* of radius R, cross section $A = \pi R^2$, length L, and volume $V = AL$. Keeping the origin at its center and assuming a constant speed for the longitudinal expansion we have

$$R = R_i, \quad A = A_i, \quad L = L_i t/t_i, \quad V = V_i t/t_i, \quad (43)$$

where the suffix i labels *initial* values. The ansatz (4) of the velocity profile reads

$$\boldsymbol{v} = z\hat{e}_z/t; \qquad -L/2 \le z \le +L/2, \quad (44)$$

subject to the restriction that the speed at the edges $\pm L/2$ must be less than c, i.e.,

$$\frac{L}{2t} = \frac{L_i}{2t_i} < 1. \quad (45)$$

Production configuration of J/ψ

Employing cylindrical coordinates let a typical ψ meson be created at the instant t_I, having position $\boldsymbol{x}_\psi{}^I$, and with transverse velocity $\boldsymbol{v}_\psi{}^I$ (in the mid-rapidity region) such that

$$\begin{aligned} t_I &= t_i + \gamma_\psi \tau_{\rm F}; \qquad \boldsymbol{x}_\psi{}^I = \left(\boldsymbol{r}_\psi{}^I, z_\psi^I\right) = \left(r_\psi^I, \phi_\psi^I, z_\psi^I\right), \\ \boldsymbol{v}_\psi{}^I &= \boldsymbol{v}_\psi = \left(\boldsymbol{v}_\psi{}^{\rm T}, 0\right) = (v_{\rm T}, 0, 0), \\ F &= \boldsymbol{v}\cdot\hat{v}_\psi = (z\hat{e}_z/t)\cdot\hat{v}_\psi^{\rm T} = 0, \end{aligned} \quad (46)$$

where $\tau_{\rm F} \approx 0.89\,{\rm fm}/c$ is the *formation* time of the bound state in the $c\bar{c}$ barycentric frame. Of course, the concept of formation time was not utilized while drawing the graphs 1–8 in Sect. 4.

Kinematics of J/ψ trajectory

The position 3-vector at a general instant t becomes

$$\boldsymbol{x}_\psi \equiv [\boldsymbol{r}_\psi, z_\psi] = \left[\boldsymbol{r}_\psi{}^I + (t - t_I)\boldsymbol{v}_\psi{}^{\rm T}, z_\psi^I\right]. \quad (47)$$

The transverse trajectory will hit the cylinder of radius $R = R_I$ after a time interval t_{R_I} by covering a distance d_{R_I} such that

$$\begin{aligned} |\boldsymbol{r}_\psi{}^I + t_{R_I}\boldsymbol{v}_\psi{}^{\rm T}| = R_I; \qquad t_{R_I} &= d_{R_I}/v_{\rm T}, \\ d_{R_I} &= -r_\psi^I\cos\phi_\psi^I + \sqrt{R_I^2 - r_\psi^{I\,2}\sin^2\phi_\psi^I}. \end{aligned} \quad (48)$$

In the fireball frame the full temporal range of our interest is obviously

$$t_I \le t \le t_{II}; \qquad t_{II} = \min(t_I + t_{R_I}, t_{\rm life}). \quad (49)$$

This prescription was also utilized in [9] and it improves the work of [8] by incorporating the formation time.

Formulation of $S(p_{\rm T})$

Let us return to the modified dissociation rate derived in Sect. 4. The value $F = 0$ (cf. (46)) greatly simplifies the kinematics of (30). Furthermore, since the time-space point x in (21) is to be chosen on the J/ψ *trajectory* itself, the notation $\langle\tilde{\Gamma}(x)\rangle$ of (34) is equivalent to

$$\langle\tilde{\Gamma}[t]\rangle \equiv \langle\tilde{\Gamma}\left(t, p_{\rm T}, z_\psi^I\right)\ \rangle. \quad (50)$$

This depends parametrically on z_ψ^I in view of the longitudinal flow profile (44), and the upper limit t_{II} (cf. (49)) of the time variable depends on the production configuration r_ψ^I, ϕ_ψ^I. Then by the law of radioactive decay without recombination the effective survival probability of a chosen ψ meson will be given by the exponential ${\rm e}^{-W}$ with

$$W = \int_{t_I}^{t_{II}} {\rm d}t\ n_g[t]\ \langle\tilde{\Gamma}[t]\rangle. \quad (51)$$

Upon averaging ${\rm e}^{-W}$ over the production configuration of the ψ's we arrive at the final expression for the net survival probability:

$$\begin{aligned} S(p_{\rm T}) = \int_{V_I} {\rm d}^3x_\psi^I \left(R_I^2 - r_\psi^{I\,2}\right){\rm e}^{-W} \\ \Big/ \int_{V_I} {\rm d}^3x_\psi^I \left(R_I^2 - r_\psi^{I\,2}\right), \\ {\rm d}^3x_\psi^I = {\rm d}r_\psi^I\ r_\psi^I\ {\rm d}\phi_\psi^I\ {\rm d}z_\psi^I. \end{aligned} \quad (52)$$

Remarks

This is a new result showing that due to the inhomogeneity introduced by the ensuing longitudinal expansion the spatial integration in (52) must extend over the *volume* $V_I = V_i t_I/t_i$ available at the instant of creation. Hence the entry concerning the *initial* length L_i and radius R_i of the plasma becomes essential in Table 2. However, in the *absence* of collective flow the integral needs to run only over the cross sectional *area* A_I of the fireball as was done in [8,9].

Table 2. Colliding nuclei, collision energy, initial length of cylindrical QGP, and its radius at RHIC(1) and LHC(1). The length is assumed to lie in the range $0.1 \le L_i \le 1\,{\rm fm}$ since the sea-quarks of the nucleon are spread over a distance of order $\Lambda \approx 1\,{\rm fm}$. [We do not use the L_i corresponding to directly Lorentz-contracted, disc-shaped nuclei to avoid too large or too small values.]

	Nuclei	Energy ($\sqrt{s}$) (GeV/nucleon)	L_i (fm)	R_i (fm)
RHIC(1)	^{197}Au	200	$0.1 \le L_i \le 1$	6.98
LHC(1)	^{208}Pb	5000	$0.1 \le L_i \le 1$	7.01

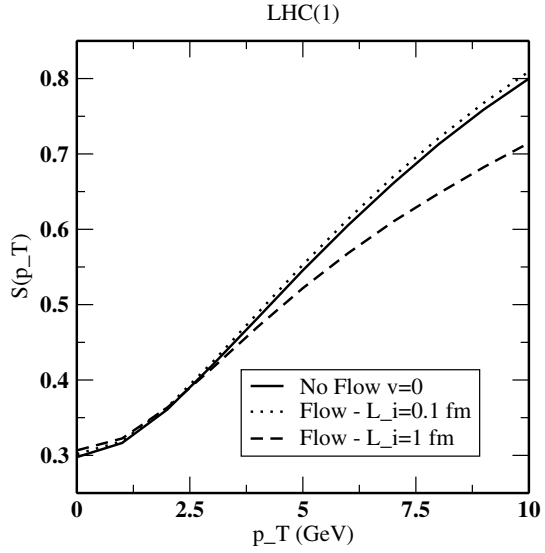

Fig. 9. The survival probability of J/ψ in an equilibrating parton plasma at LHC energy with initial conditions given in Table 1. The solid curve is the result of [9], i.e., in the *absence of flow* while the dotted and dashed curves represent the survival of J/ψ when the plasma is undergoing longitudinal expansion with the initial values of the length of the cylinder $L_i = 0.1\,\mathrm{fm}$ and 1 fm, respectively

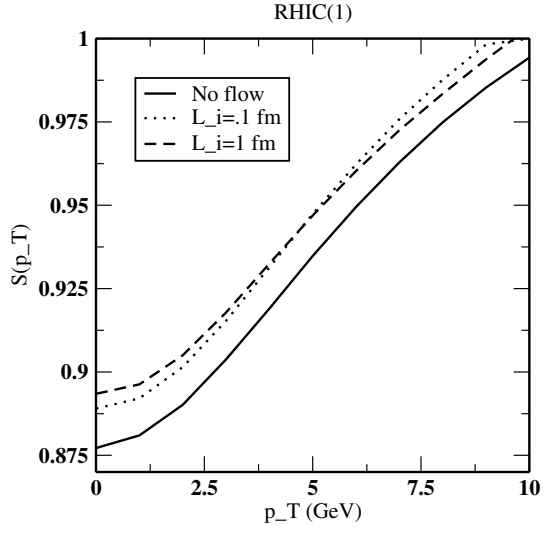

Fig. 10. Same as Fig. 9 but computed for RHIC initial conditions

Numerical illustration

As pointed out in [9] the precise value of the ψ meson formation time τ_F is ambiguous; however we adopt $\tau_\mathrm{F} \simeq 0.89\,\mathrm{fm}/c$ as a fair representative. For the chosen creation configuration of the ψ meson the function W was first computed from (51) and then the survival probability was numerically evaluated using (52). Figures 9 and 10 show the dependence of $S(p_\mathrm{T})$ on the transverse momentum corresponding to the LHC(1) and RHIC(1) initial conditions, respectively (cf. Tables 1 and 2). The dotted ($L_i = 0.1\,\mathrm{fm}$) and dashed ($L_i = 1\,\mathrm{fm}$) curves are computed in the *presence* of longitudinal flow while the solid curve is borrowed from [9] in the *absence* of hydrodynamic flow profile. The main features of these graphs may be explained as follows.

Interpretation

(i) In the absence of flow, i.e., for $v = 0$, the $S(p_\mathrm{T})$ solid lines in Figs. 9 and 10 rise steadily with p_T. This is because $\langle\tilde{\Gamma}\rangle$ of Fig. 4, and hence the W integral of (51), diminish with p_T.
(ii) In the presence of flow with a small initial length $L_i \sim 0.1\,\mathrm{fm}$ the $S(p_\mathrm{T})$ dotted curves in Figs. 9 and 10 are slightly above the solid line. To explain this, we note that the flow profile $v = z/t$ remains non-relativistic over short lengths and the destructive interference between the I_0 and I_1 terms in (36) becomes slightly stronger (compared to the $v = 0$ case). The consequent drop of $\langle\tilde{\Gamma}\rangle$ or W pushes $S(p_\mathrm{T})$ upwards.
(iii) In the presence of flow with a large initial length of $L_i = 1\,\mathrm{fm}$ the $S(p_\mathrm{T})$ dashed curve lies below the solid line in the LHC case (cf. Fig. 9) but lies above the solid line in RHIC case (cf. Fig. 10).
(iv) To explain this peculiar contrast between Figs. 9 and 10 we note that as the expanding cylinder becomes much bigger than 1 fm the flow profile $v = z/t$ may become relativistic over a substantial part of its length so that the graphs of Fig. 8 can be employed. At higher temperatures ($0.8 < T < 0.6$, say) at LHC the $\langle\tilde{\Gamma}\rangle$ curves are known to drop with increasing p_T. But at lower temperatures ($0.6 < T < .2$), say) at RHIC the $\langle\tilde{\Gamma}\rangle$ curves rise with p_T in Fig. 8 whereby a contrast occurs.
(v) Of course, the relative shift in $S(p_\mathrm{T})$ due to longitudinal flow is only about 10% to 15% even at $p_\mathrm{T} = 10\,\mathrm{GeV}$.

6 Conclusions

(a) In this paper we have extended our earlier work [9] by explicitly including the effect of a hydrodynamic expansion profile on the gluonic dissociation of J/ψ's created in an equilibrating QGP. The treatment of Sects. 3 and 4 is very general in the sense that both the fluid velocity $\boldsymbol{v}$ and the ψ momentum $\boldsymbol{p}_\psi$ are arbitrary. Only in Sect. 5 we specialize to a longitudinal fluid expansion and transverse motion of ψ.
(b) Our theoretical formulae for the gluon number density n_g (cf. (11)), modified g–ψ break-up rate $\langle\tilde{\Gamma}\rangle$ (cf. (34)), and the survival probability of ψ, S (cf. (52)), are new. These are derived by making careful Lorentz transformations between the rest frames of the fireball, plasma, and ψ meson.
(c) At specified fugacity λ_g the effect of the flow velocity $\boldsymbol{v}$ is to increase the number density of hard gluons (which are primarily responsible for breaking the J/ψ's) as shown in the numerical estimate (12).
(d) Our expression (32) and (34) of $\langle\tilde{\Gamma}(x)\rangle$ contains partial wave contributions called I_0 and I_1 whose mutual interference is controlled by the anisotropic $\cos\theta_{\psi w}$ factor. This significantly affects the variation of $\langle\tilde{\Gamma}\rangle$ with T, p_T and $\boldsymbol{v}$ as depicted in Figs. 3–8.

(e) The presence of a longitudinal expansion pushes up the graph of $S(p_{\rm T})$ compared to the $v \equiv 0$ case for non-relativistic flow appropriate to a small initial length of $L_i = 0.1\,{\rm fm}$.
(f) However, in the case of relativistic longitudinal flow appropriate to a larger initial length of $L_i = 1\,{\rm fm}$ the downward shift of $S(p_{\rm T})$ graph at LHC is in sharp contrast to the upward shift at RHIC. Such a contrast between the behaviors at LHC and RHIC is caused by the different initial temperatures generated therein. The relative shift is, however, is only 10%–15% even at $p_{\rm T} = 10\,{\rm GeV}$.
(g) In a future communication we plan to study the detailed effect of a transverse expansion of the medium on $S(p_{\rm T})$. It is expected that there will be a more rapid cooling with time and also possibly constructive interference in (35).

Acknowledgements. VJM thanks the UGC, government of India, New Delhi for financial support. We thank Dr. Dinesh Kumar Srivastava for useful discussions during this work.

Appendix

Evaluation of the integral (28)

Our derivation proceeds through the following steps.

First step

We recall the symbols (30) and (31); we work in the ψ meson rest frame, and rewrite (29) as

$$\langle \Gamma(x)\rangle = \frac{2}{\pi^3 n_g}\int_1^\infty \epsilon_\psi^3 {\rm d}Q^0 {Q^0}^2 \int_0^{4\pi} {\rm d}\Omega_{q\psi}\ \gamma_\psi \left[\ 1+|\boldsymbol{v}_\psi|\cos\theta_{q\psi}\ \right] \times \sigma_{\rm Rest}\sum_{n=1}^\infty \lambda_g^n {\rm e}^{-C_n Q^0+\rho_n\cos\theta_{qw}}. \quad (A.1)$$

Second step

Next, a partial wave expansion is done of the exponential

$$\begin{aligned} {\rm e}^{\rho_n\cos\theta_{qw}} &= \sum_{l=0}^\infty {\rm i}^l j_l(-{\rm i}\rho_n)(2l+1)P_l(\cos\theta_{qw}) \quad (A.2)\\ &= \sum_{l=0}^\infty I_l(\rho_n) 4\pi \sum_{m=-l}^{l} {Y_l^m}^*(\Omega_{q\psi})Y_l^m(\Omega_{\psi w}). \end{aligned}$$

Here $\rho_n = D_n Q^0$ as before, j_l denotes the spherical Bessel functions, $I_l(\rho_n) = {\rm i}^l j_l(-{\rm i}\rho_n)$, the addition theorem has been used for the Legendre polynomial $P_l(\cos\theta_{qw})$, and $\Omega_{\psi w}$ are the polar angles of $\hat{v}_\psi$ with respect to the local flow direction $\hat{w}$.

Third step

Next, the relevant angular integral appearing in (A.1) and (A.2) reads

$$\int_0^{4\pi} {\rm d}\Omega_{q\psi}\ \left[\ 1+|\boldsymbol{v}_\psi|\cos\theta_{q\psi}\ \right] {Y_l^m}^*(\Omega_{q\psi}) = \sqrt{4\pi}\left[\delta_{l0}+\sqrt{\frac{1}{3}}|\boldsymbol{v}_\psi|\delta_{l1}\right]\delta_{m0}, \quad (A.3)$$

due to the orthogonality of spherical harmonics.

Fourth step

Finally, inserting the informations (A.2) and (A.3) back into the starting expression (A.1) we obtain

$$\langle \Gamma(x)\rangle = \frac{2}{\pi^3 n_g}\int_1^\infty \epsilon_\psi^3 {\rm d}Q^0 {Q^0}^2 \gamma_\psi\ \sigma_{\rm Rest}\sum_{n=1}^\infty \lambda_g^n {\rm e}^{-c_n Q^0} \times 4\pi\sum_{l=0}^\infty I_l(\rho_n)\left[\delta_{l0}+\sqrt{\frac{1}{3}}|\boldsymbol{v}_\psi|\delta_{l1}\right]\sqrt{4\pi}Y_l^0(\Omega_{\psi w}), \quad (A.4)$$

which indeed coincides with (32) of the text.

References

1. Helmut Satz, Rept. Prog. Phys. **63**, 1511 (2000)
2. T. Matsui, H. Satz, Phys. Lett. B **178**, 416 (1986)
3. B.K. Patra, D.K. Srivastava, Phys. Lett. B **505**, 113 (2001)
4. D. Kharzeev, H. Satz, Phys. Lett. B **334**, 155 (1994)
5. D. Kharzeev, H. Satz, Phys. Lett B **366**, 316 (1996)
6. B.K. Patra, V.J. Menon, Nucl. Phys. A **708**, 353 (2002)
7. R.L. Thews, M. Schroedter, J. Rafelski, Phys. Rev. C **63**, 054905 (2001)
8. Xiao-Ming Xu, D. Kharzeev, H. Satz, Xin-Nian Wang, Phys. Rev. C **53**, 3051 (1996)
9. B.K. Patra, V.J. Menon, Eur. Phys. J. C **37**, 115 (2004)
10. T.S. Biro, E. van Doorn, M.H. Thoma, B. Müller, X.-N. Wang, Phys. Rev. C **48**, 1275 (1993)
11. D.K. Srivastava, M.G. Mustafa, B. Müller, Phys. Rev. C **56**, 1064 (1997)
12. D. Pal, B.K. Patra, D.K. Srivastava, Eur. Phys. J. C **17**, 179 (2000)
13. Jean-Yves Ollitrault, Phys. Rev. D **46**, 229 (1992)
14. Xin-Nian Wang, Feng Yuan, Phys. Lett. B **540**, 62 (2002)
15. X.-N Wang, M. Gyulassy, Phys. Rev. D **44**, 3501 (1991)
16. M.E. Peskin, Nucl. Phys. B **156**, 365 (1979); G. Bhanot, M.E. Peskin, Nucl. Phys. B **156**, 391 (1979)
17. C. Gerschel, J. Hüfner, Phys. Lett. B **207**, 253 (1988)